

# Supporting Information: Stoichiometry dependent phase evolution of co-evaporated formamidinium and cesium lead halide thin films

Karl L. Heinze<sup>a</sup>, Patrick Wessel<sup>a</sup>, Melissa Mauer<sup>a</sup>, Roland Scheer<sup>a</sup>, and Paul Pistor<sup>a,b,\*</sup>

<sup>a</sup>Thin Film Photovoltaics, Institute of Physics, MLU Halle-Wittenberg, Halle (Saale) 06120, Germany

<sup>b</sup>Universidad de Pablo de Olavide, Carretera de Utrera 1, 41013, Sevilla, Spain

\*ppis@upo.es

This Supporting Information provides additional information to complement the main manuscript on  $(\text{Cs,FA})\text{Pb}(\text{I,Br})_3$  perovskite evaporation at room temperature. The herein shown figures and tables are each referenced in the manuscript. Each respective figure is explained in the given caption.

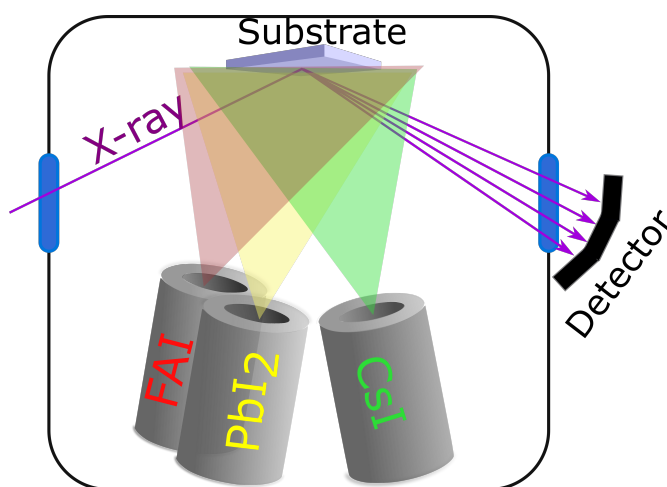


**Figure S1.** Schematic representation of our high vacuum chamber with *in situ* X-ray diffraction (XRD) system. The x-ray enters the chamber from the left and is diffracted onto the planar detector on the right by the sample.

Sample	Cs	Pb	I	Br	X/Pb	Cs/FA	Br/I
High	4.3	19.6	67.2	9.0	3.89	0.13	0.13
Med	4.1	23.4	58.3	14.2	3.09	0.19	0.24
Low	4.4	26.3	57.7	11.6	2.64	0.36	0.2

**Table S1.** Atomic contents in % and respective X/Pb, Cs/FA and Br/I ratios of high, medium and low X/Pb samples.

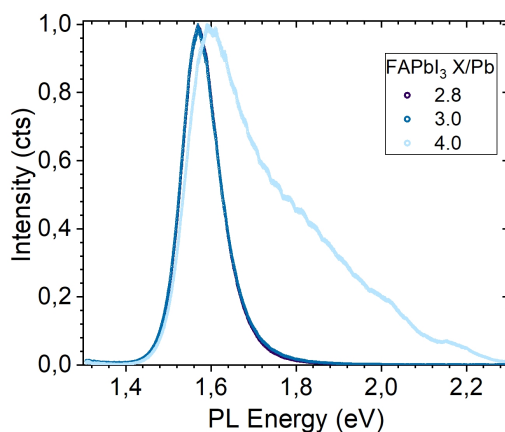


**Figure S2.** Photoluminescence (PL) measurements of FAPbI<sub>3</sub> absorbers with X/Pb of 2.8, 3 and 4 after storage in air for one week are shown. The peaks at 1.57 eV for the I/Pb of 2.8 and 3 correspond well to the  $\alpha$ - $\delta$  phase junction observed by Ma et al.<sup>1</sup>. They observed two perovskite phases for FAPbI<sub>3</sub> via XRD and only one peak at 1.51 eV (hence just one phase) during PL measurements, positioned between  $\alpha$  and  $\delta$  phase peaks at 1.47 eV and around 2.43 eV, respectively<sup>1</sup>. This seems to also be the case for the samples shown here. The sample with I/Pb of 4 possesses a main peak at 1.6 eV with a long tail towards higher PL energies. A possible explanation for this tail could be the formation of amorphous phases or Ruddlesden-Popper FA<sub>n+1</sub>Pb<sub>n</sub>I<sub>3n+1</sub> compounds, that have been observed to exhibit similar PL behavior<sup>2</sup>. Peak positions in comparison to (Cs,FA)PbI<sub>3</sub> and (Cs,FA)Pb(I,Br)<sub>3</sub> absorbers are shown in fig. S5. Interpretation of the PL measurements in conjunction with the measurements in the main manuscript is limited, since the latter were done under N<sub>2</sub> atmosphere and vacuum, but the reaction of the unencapsulated layers with the environment could not have been prevented previous to the PL measurements.

1 F. Ma, Chemical Science, 2017, 8, 800–805 2 B. A. Rosales, Nature Communications, 2020, 11, 5234

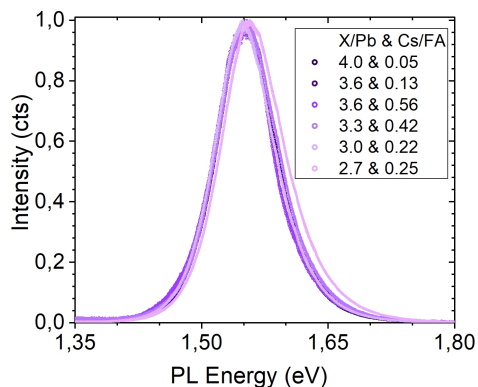


**Figure S3.** PL measurements on (Cs,FA)PbI<sub>3</sub> absorbers after storage in air for one week. Across all shown compositions, the peak position remained at 1.55 eV. Only the layer with I/Pb of 2.7 exhibits a slight blueshift to 1.56 eV. These PL positions hint towards a similar  $\alpha$ - $\delta$  phase junction as described below fig. S2. The main peaks' positions in comparison with FAPbI<sub>3</sub> and (Cs,FA)Pb(I,Br)<sub>3</sub> are displayed in fig. S5 Interpretation of the PL measurements in conjunction with the measurements in the main manuscript is limited, since the latter were done under N<sub>2</sub> atmosphere and vacuum, but the reaction of the unencapsulated layers with the environment could not have been prevented previous to the PL measurements.

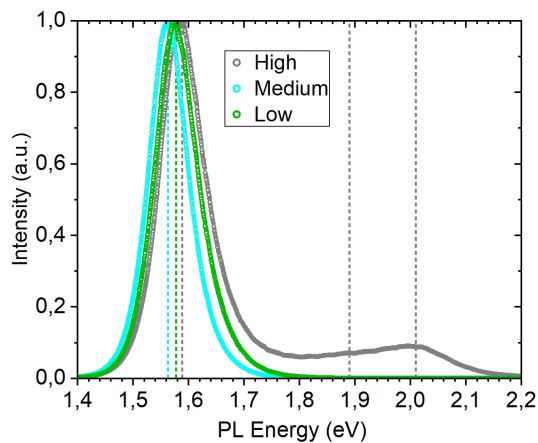


**Figure S4.** PL measurements on  $(\text{Cs,FA})\text{Pb}(\text{I,Br})_3$  absorbers after storage in air for one week are shown. Respective atomic compositions for the samples with high, medium and low X/Pb are displayed in table S1. The sample with high X/Pb exhibits the highest main PL peak energy at 1.59 eV and two small peaks at 1.89 and 2.02 eV. This could be caused by some halide phase segregation during storage in air, or by the the formation of Ruddlesden-Popper compounds as discussed above. The low X/Pb sample displays a peak at 1.58 eV and the medium X/Pb sample's peak is at 1.56 eV. All main peaks' positions in comparison with  $\text{FAPbI}_3$  and  $(\text{Cs,FA})\text{PbI}_3$  are displayed in fig. S5. Interpretation of the PL measurements in conjunction with the measurements in the main manuscript is limited, since the latter were done under  $\text{N}_2$  atmosphere and vacuum, but the reaction of the unencapsulated layers with the environment could not have been prevented previous to the PL measurements.

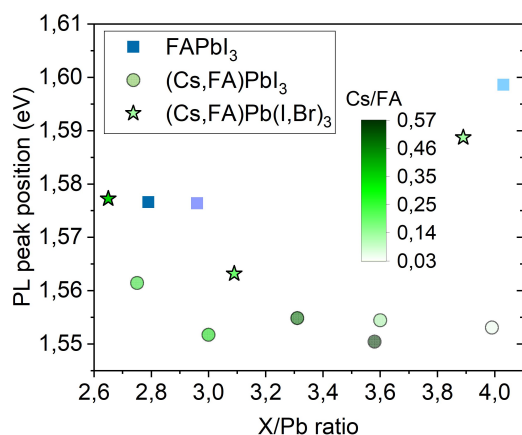


**Figure S5.** Main peak positions for  $\text{FAPbI}_3$ ,  $(\text{Cs,FA})\text{PbI}_3$  and  $(\text{Cs,FA})\text{Pb}(\text{I,Br})_3$  displayed in fig. S2, S3 and S4, respectively.

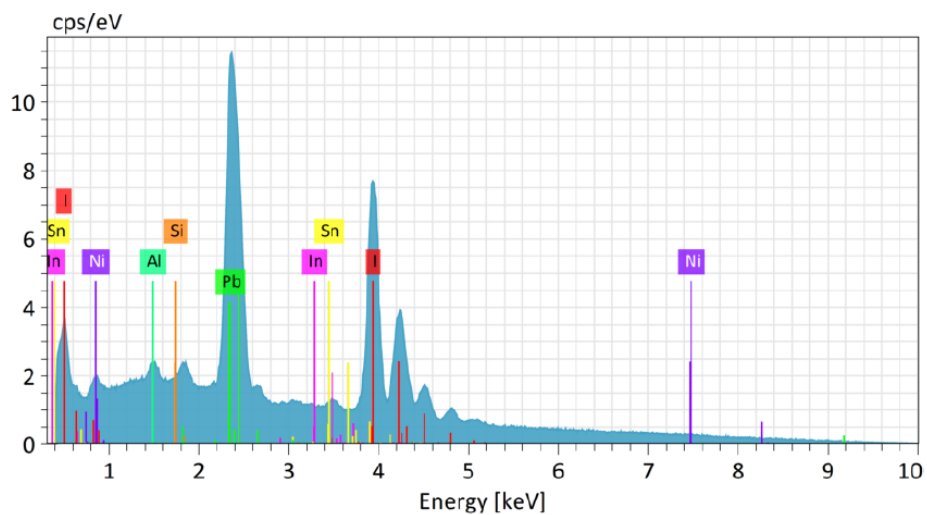


**Figure S6.** Exemplary EDX spectrum of a  $\text{FAPbI}_3$  sample with an I/Pb ratio of 2.8.

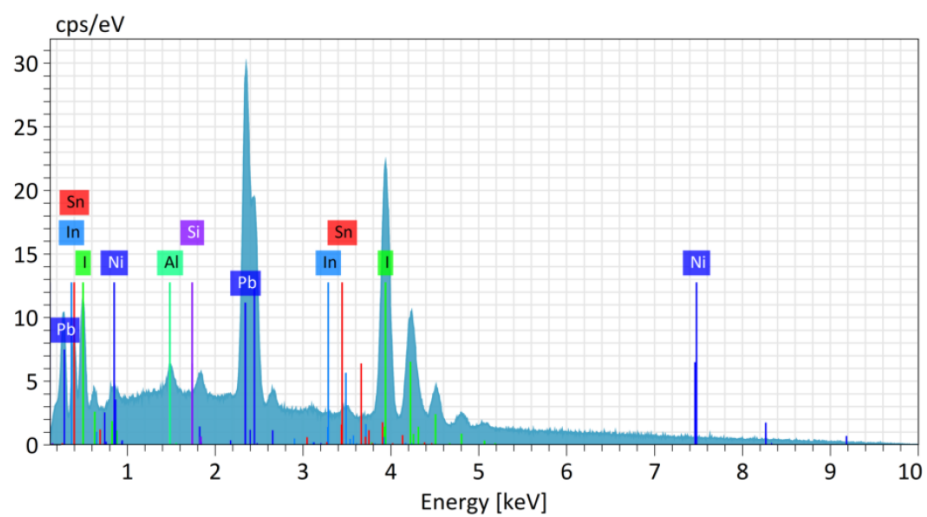


**Figure S7.** Exemplary EDX spectrum of a  $\text{FAPbI}_3$  sample with I/Pb of 3.0.

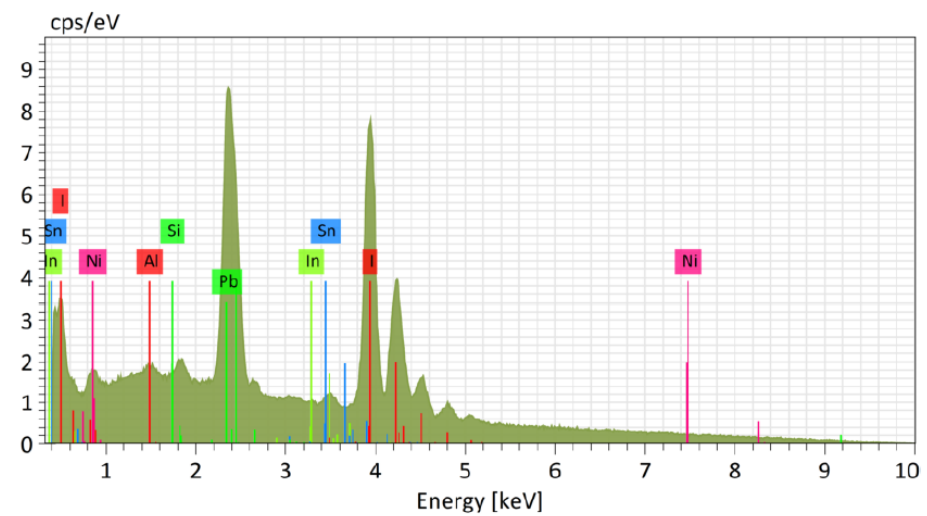


**Figure S8.** Exemplary EDX spectrum of a  $\text{FAPbI}_3$  sample with I/Pb of 3.8.

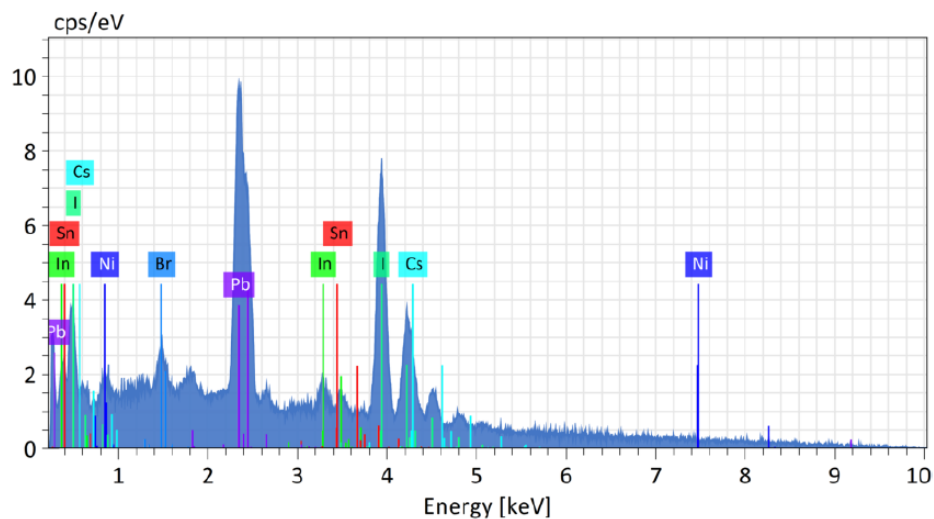


**Figure S9.** Exemplary EDX spectrum of a  $(\text{Cs,FA})\text{PbI}_3$  sample with I/Pb of 2.7 and Cs/FA of 0.05.

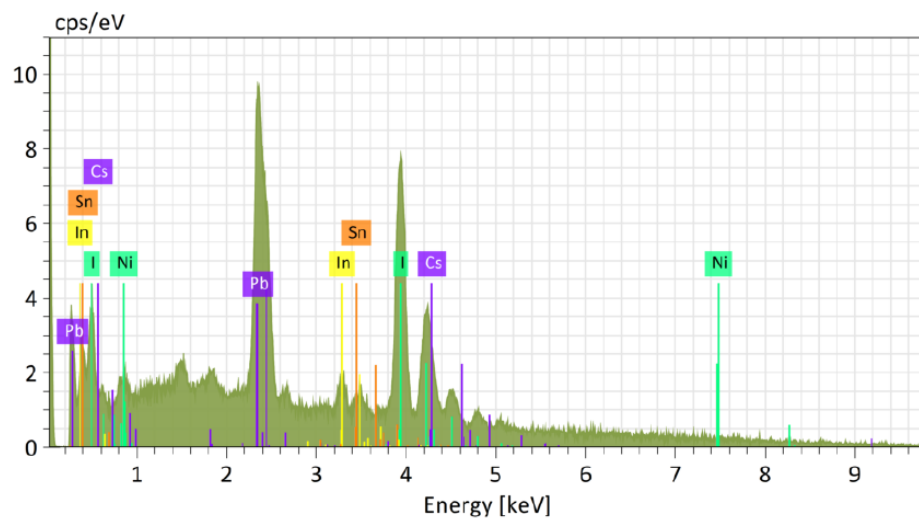


**Figure S10.** Exemplary EDX spectrum of a  $(\text{Cs,FA})\text{PbI}_3$  sample with I/Pb of 3.1 and Cs/FA of 0.05.

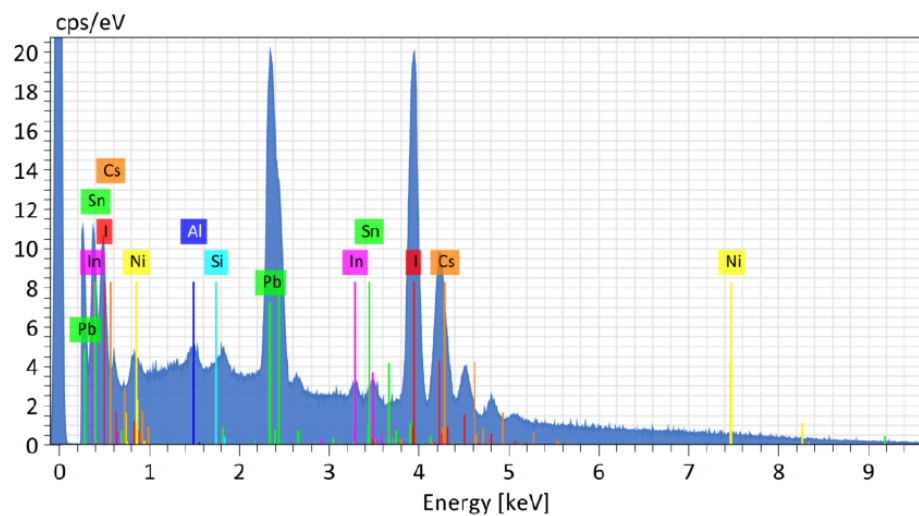


**Figure S11.** Exemplary EDX spectrum of a  $(\text{Cs,FA})\text{PbI}_3$  sample with I/Pb of 4.1 and Cs/FA of 0.11.

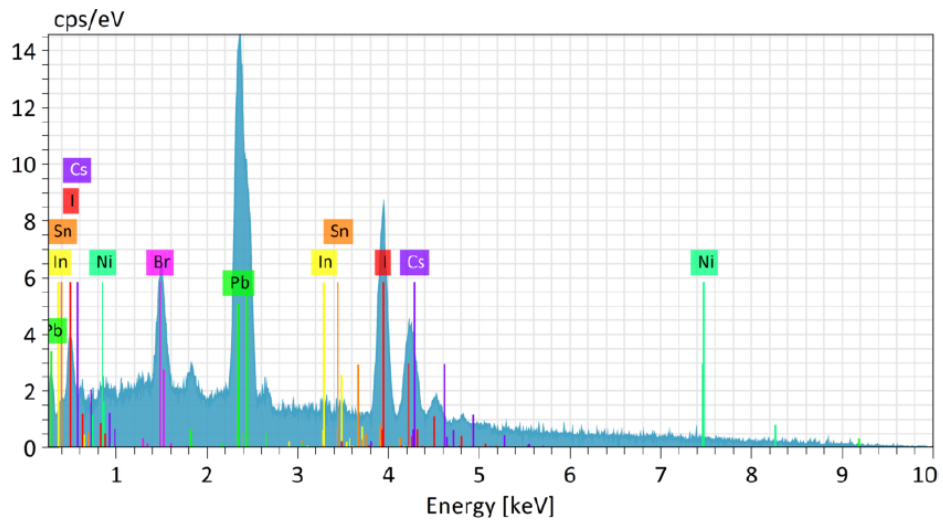


**Figure S12.** EDX spectrum of a  $(\text{Cs,FA})\text{Pb}(\text{I,Br})_3$  sample with X/Pb of 2.65, Cs/FA of 0.36 and Br/I of 0.2. X is the combined halide content of Br and I.

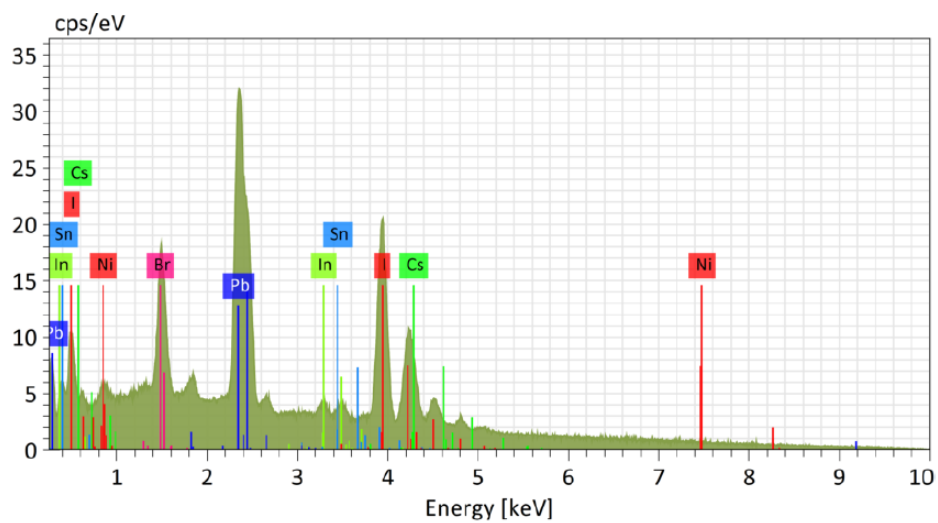


**Figure S13.** EDX spectrum of a  $(\text{Cs,FA})\text{Pb}(\text{I,Br})_3$  sample with an X/Pb of 3.09, Cs/FA of 0.19 and Br/I of 0.24. X is the combined halide content of Br and I.

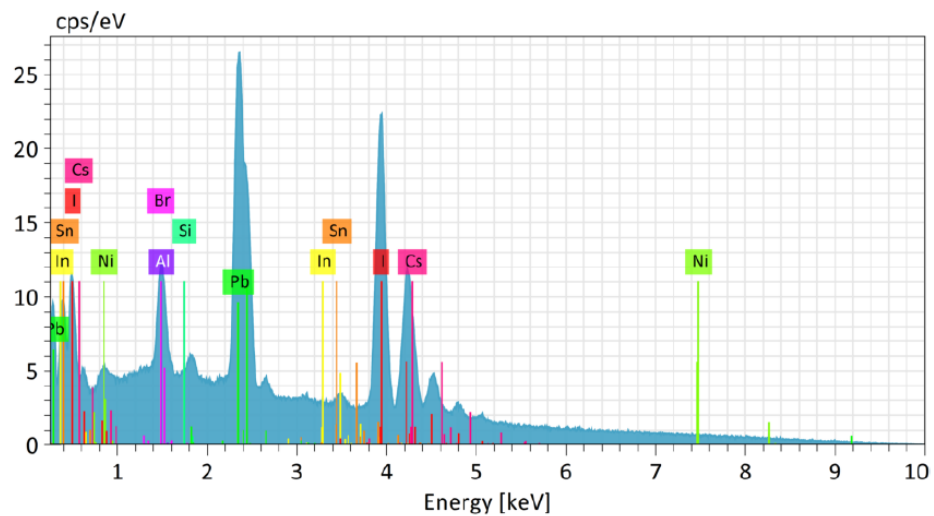


**Figure S14.** EDX spectrum of a  $(\text{Cs,FA})\text{Pb}(\text{I,Br})_3$  sample with an X/Pb of 3.89, Cs/FA of 0.13 and Br/I of 0.14. X is the combined halide content of Br and I.

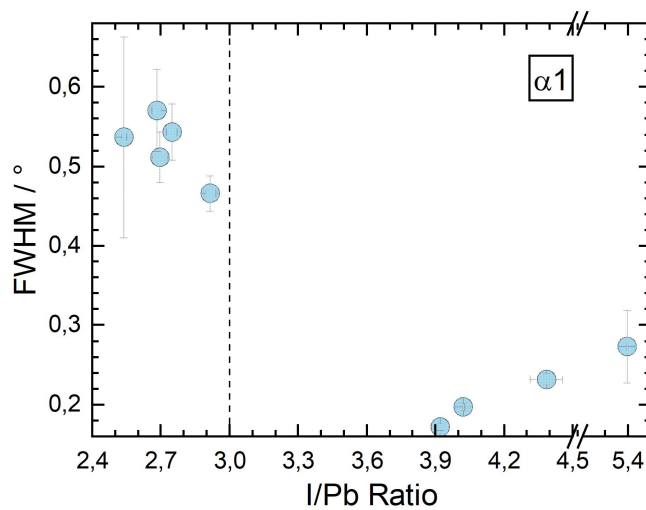


**Figure S15.** Course of the  $\alpha_1$  FWHM depending on the I/Pb ratio in  $\text{FAPbI}_3$  absorbers. A minimum is observed at I/Pb of 3.9.

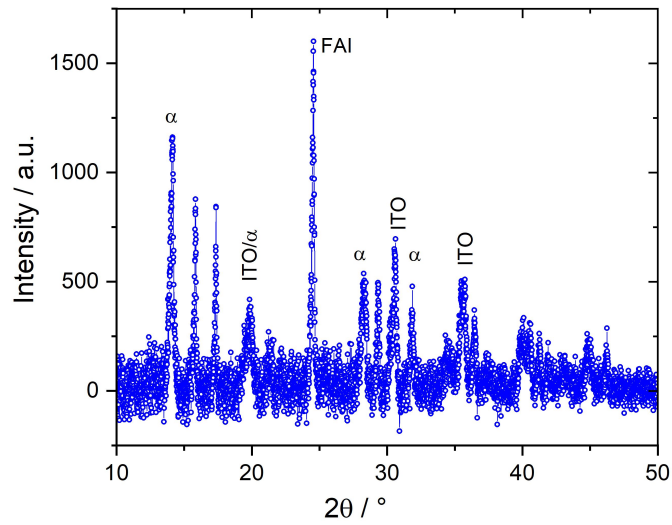


**Figure S16.**  $\theta$ - $\theta$  scan of a FAPbI<sub>3</sub> absorber with I/Pb of 5.4 showing a large FAI peak at 24.5°. FAPbI<sub>3</sub>  $\alpha$  phase and ITO peaks are marked accordingly.

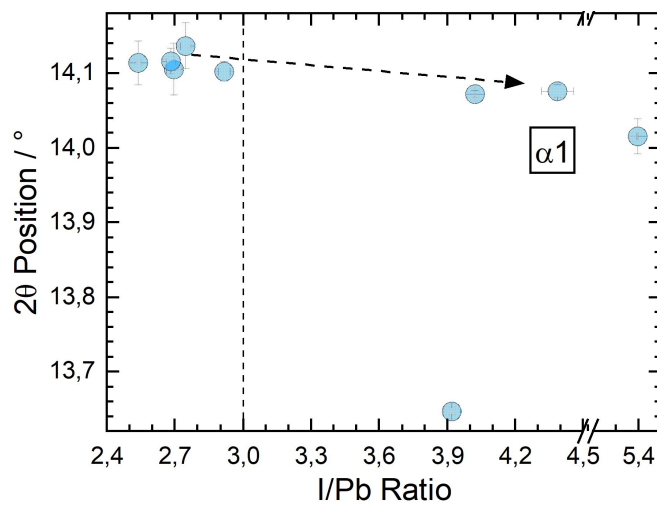


**Figure S17.**  $\alpha_1$  peak positions for different I/Pb ratios in FAPbI<sub>3</sub> absorbers. The off-position at an I/Pb of 3.9 results from a decalibration in the XRD setup, which leads to a shift in peak position, but otherwise the same peak properties.



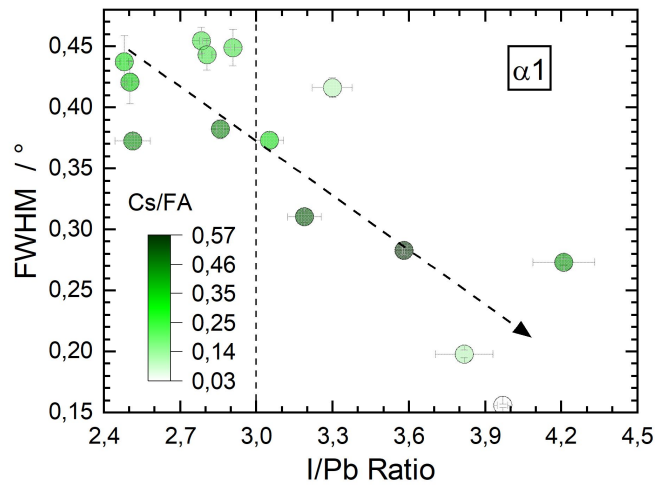


**Figure S18.** Course of the  $\alpha_1$  FWHM depending on the I/Pb ratio in (Cs,FA)PbI<sub>3</sub> absorbers. As was seen in fig. S15 for FAPbI<sub>3</sub>, a minimum occurs at I/Pb of 3.9.

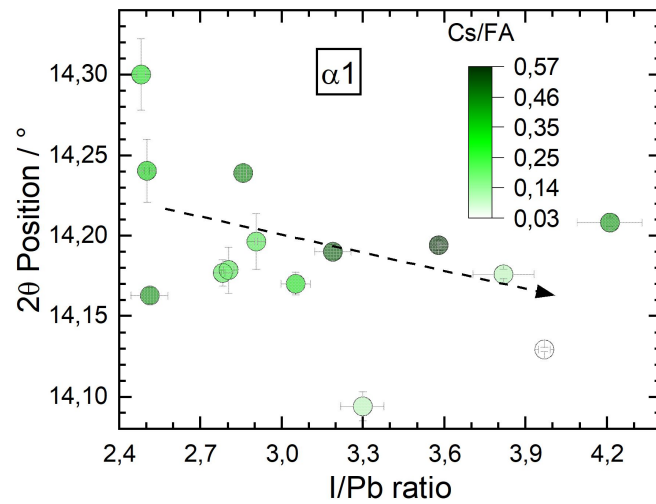


**Figure S19.** The course  $\alpha_1$  peak for varying I/Pb and Cs/FA ratios. Although the peaks are clearly shifted to a higher average angle of around 14.2° in comparison to 14.1° for FAPbI<sub>3</sub>, no obvious dependence is visible between I/Pb and the position of 2θ for  $\alpha_1$ .

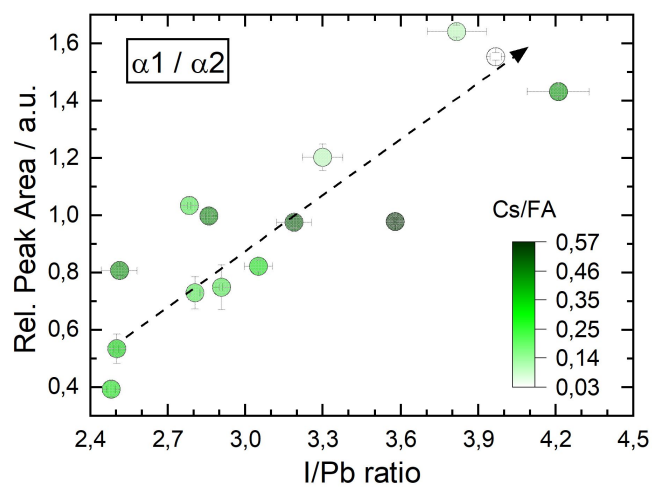


**Figure S20.** Rel. peak areas of  $\alpha_1$  and  $\alpha_2$  in  $(\text{Cs,FA})\text{PbI}_3$  at  $14^\circ$  and  $28^\circ$ , respectively, plotted against the respective I/Pb ratios.

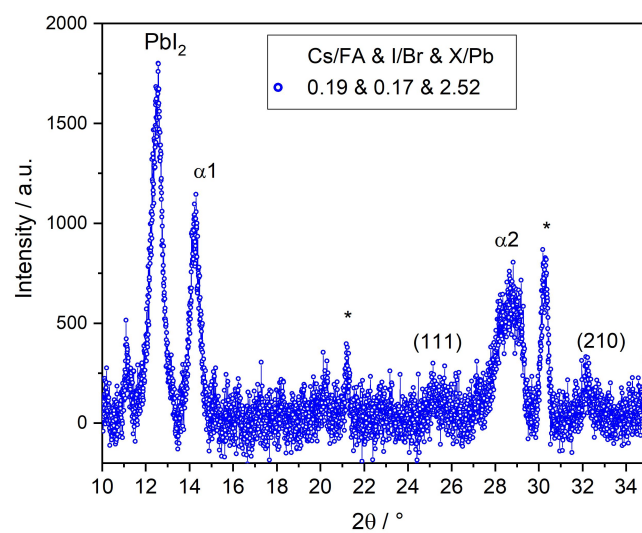


**Figure S21.**  $\theta$ - $\theta$  scan of a  $(\text{Cs,FA})\text{Pb}(\text{I,Br})_3$  layer with an X/Pb ratio of 2.54.

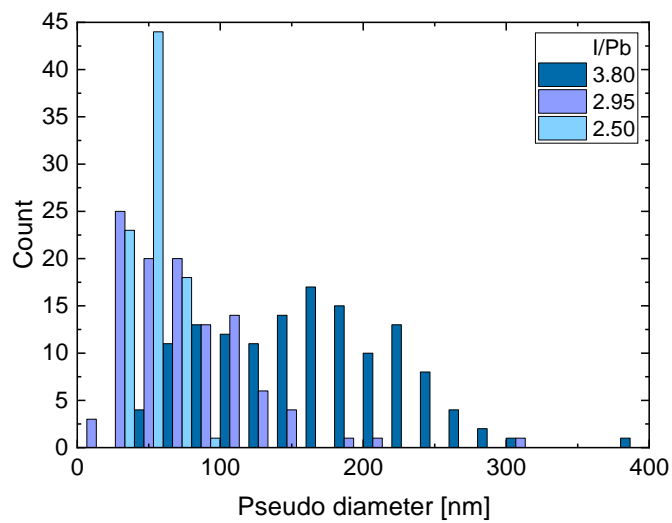


**Figure S22.** Grain size distribution of  $\text{FAPbI}_3$  with a I/Pb ratio of 2.50, 2.95, and 3.80 with an average pseudo diameter of 48.7, 74.2 and 164 nm. The top-view grain size distributions were calculated in ImageJ from the SEM images in Fig. 3 in the main manuscript. For comparability, the grain area was assumed to be circular. From this pseudo-circular area  $A = \pi \cdot (d/2)^2$ , the pseudo-diameter  $d$  is used for comparison.

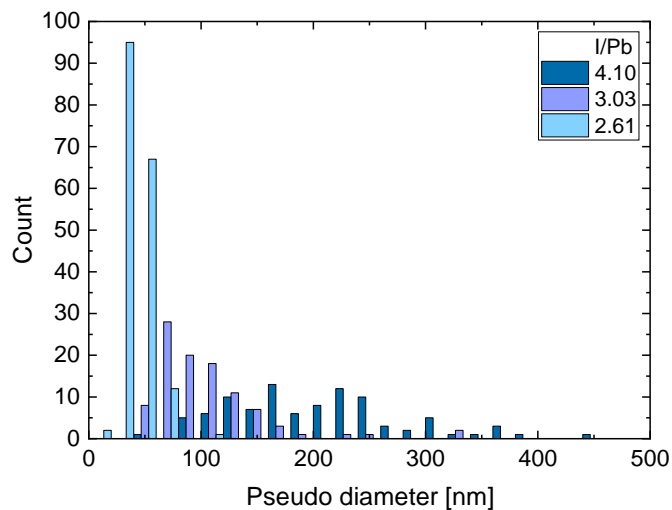


**Figure S23.** Grain size distribution of  $(\text{Cs,FA})\text{PbI}_3$  with a I/Pb ratio of 2.61, 3.03, and 4.10 with an average pseudo diameter of 39.4, 105 and 204 nm. The top-view grain size distributions were calculated in ImageJ from the SEM images in Fig. 6 in the main manuscript. For comparability, the grain area was assumed to be circular. From this pseudo-circular area  $A = \pi \cdot (d/2)^2$ , the pseudo-diameter  $d$  is used for comparison.

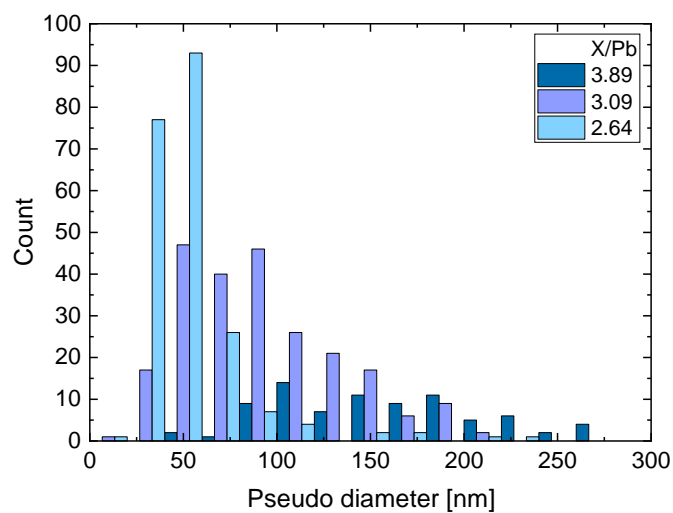


**Figure S24.** Grain size distribution of  $(\text{Cs,FA})\text{Pb}(\text{I,Br})_3$  with a X/Pb ratio of 2.64, 3.09, and 3.89 with an average pseudo diameter of 51.1, 90.8 and 156 nm. The top-view grain size distributions were calculated in ImageJ from the SEM images in Fig. 8 in the main manuscript. For comparability, the grain area was assumed to be circular. From this pseudo-circular area  $A = \pi \cdot (d/2)^2$ , the pseudo-diameter  $d$  is used for comparison.